A Vibrational Spectroscopic Study of the Fate of Oxygen-Containing Functional Groups and Trapped CO_2 in Single-Walled Carbon Nanotubes During Thermal Treatment

Xue Feng,[†,‡] Christopher Matranga,[§] Radisav Vidic,[‡] and Eric Borguet*[,†]

Chemistry Department, Temple University, Philadelphia, Pennsylvania 19122, Department of Civil and Environmental Engineering, University of Pittsburgh, Pittsburgh, Pennsylvania 15260, and National Energy Technology Laboratory, United States Department of Energy, P.O. Box 10940, Pittsburgh, Pennsylvania 15236

Received: June 15, 2004; In Final Form: August 30, 2004

The oxygen-containing functional groups, introduced by common purification procedures, on single-walled carbon nanotubes (SWNTs) made by both the HiPco and laser-ablation (Rice Tubes) techniques are studied by Fourier Transform Infrared (FTIR) spectroscopy from 90 to 1400 K under vacuum. The fate of the functional groups under heating and the physically trapped CO_2 generated from the decomposition of these functional groups are investigated. Vacuum heating to ~1300 K removes most of the oxygen-containing functionalities in the purified samples. The similarities in the infrared spectra of the Rice Tubes after a 1400 K treatment with spectra for the as-received and air/HCl treated HiPco nanotubes suggests the observation of intrinsic SWNT IR bands. Vacuum heating of nitric acid treated HiPco samples leads to the formation of a new feature, tentatively assigned to cyclic anhydride groups, in the 1850 cm^{-1} region. The cyclic anhydride groups decompose and ultimately disappear after thermal annealing to 600 K. Above 700 K, the quantity of CO_2 trapped in HNO_3 treated HiPco SWNTs decreases and trapped CO_2 is completely released from the nanotubes after 1100 K even though oxygen-containing functionalities are still present on the sample. The Rice Tubes made by the laser ablation technique retain the physically trapped CO_2 even after heating to 1400 K.

Introduction

The presence of functional groups or adsorbed oxygen species on single-walled carbon nanotubes (SWNTs) is known to affect properties of these materials.[1,2] Functionalities influence the electronic properties of SWNTs by disrupting the graphitic-like sp^2 network of carbon in the SWNTs. This disruption produces local sp^3 defects which can introduce an impurity state near the Fermi level[3] and perturb the electronic spectra of these materials.[4] The conductivity[3] and solubility[5,6] of SWNTs have also been shown to change as a result of functionalization. Ultimately, the performance of SWNTs as adsorbents,[7] catalysts,[8] capacitors,[9] microscopy tips,[10−12] and sensors[13] depends on understanding and controlling surface functionalities.

Normally, as-received nanotubes contain few heteroatom functional groups. However, during various purification steps, oxygen-containing functional groups are introduced.[14,15] Some purification procedures use aggressive oxidizers such as HNO_3, H_2SO_4, or H_2O_2 to crack the passivating carbon shells encapsulating residual catalyst particles and to remove unwanted carbons.[16−18] Newer procedures use more gentle steps which expose the catalyst by heating in moist air followed by an acid wash for catalyst removal.[19] As one might expect, the amount and type of functional groups introduced by these purification steps vary drastically with each different type of procedure employed.

This work reports Fourier Transform Infrared (FTIR) studies of the functional groups present on as-received HiPco SWNTs, HiPco samples purified by an air oxidation/HCl wash, and HiPco samples purified by HNO_3 refluxing. A sample produced by laser ablation and purified by a HNO_3/H_2SO_4 treatment is also studied to show that some of the results seen with the HiPco samples can be extended to SWNTs synthesized and purified by different methods. The fate of functionalities on the as-received and purified samples is studied during vacuum heating, as is the physically trapped CO_2 generated in the purified samples during this step.[20,21]

This paper extends previous work[20,21] to significantly higher temperatures. In particular, we find that the air/HCl treatment is as effective in reducing the metal content of HiPco samples as the HNO_3 refluxing, but it does not functionalize the samples as the HNO_3 treatment does. We also find that vacuum heating is effective in removing most of the functionalities created in HNO_3-treated HiPco samples. One surprising result from our work is that heating to ~1400 K does not release physically trapped CO_2 completely from the HNO_3/H_2SO_4-treated, laser-ablation samples, but a simple heating to ~1000 K releases the trapped CO_2 to levels below our detection limit in the HNO_3-treated HiPco samples. This result hints at the different functionalities and decomposition pathways present in these samples.

Experimental Section

Sample Preparation. SWNTs produced by the HiPco process were obtained from Carbon Nanotechnologies Incorporated as an unpurified solid. Thermogravimetric analysis (TGA) of these as-received HiPco samples showed approximately 18 wt % (grams of Fe/grams of sample × 100%) of residual iron catalyst, in agreement with a previous report for these samples.[22]

The as-received HiPco SWNTs were purified by a procedure reported in the literature.[22] This included flowing moist air (0.2

* To whom correspondence should be addressed. E-mail: eborguet@temple.edu. Phone: 215-204-9696. Fax:215-204-9530.
[†] Temple University.
[‡] University of Pittsburgh.
[§] United States Department of Energy.

10.1021/jp047410k CCC: $27.50
Published on Web 12/02/2004

L/min) through the samples for 4 h at 498 K in a quartz tube furnace. Then the nanotubes were sonicated in a 3 M HCl solution for another 4 h. After acid extraction, the nanotubes were filtered and rinsed with deionized water until the rinsing water was pH neutral. The samples were dried and dispersed in toluene by sonication. TGA of the samples showed that the residual Fe content is approximately 5 wt %.

A second purification procedure was used for the HiPco samples that involved refluxing the as-received HiPco materials in 3 M HNO_3 for 8 h and allowing the samples to sit unheated in the nitric acid solution overnight with continued refluxing for another 8 h on the following day.[21] The sample was then rinsed with deionized water until the rinsing water was pH neutral and the still damp samples were dispersed in acetone. TGA of these samples showed approximately 3 wt % of residual iron.

SWNTs prepared by the laser-ablation technique were purchased from Tubes@Rice as a "Purified Grade" suspended in toluene, which are referred to as "Rice Tubes" in this study. These tubes were oxidized/purified by a nitric acid and sulfuric acid mixture by the manufacturer.[23] TGA analysis showed that the residual metal content of these materials is approximately 8 wt % of a 1:1 mixture of Ni and Co.[24]

Experimental Setup. A stainless steel ultrahigh vacuum (UHV) cell was set up for the infrared study. A turbo molecular pump (Leybold, Turbovac151) backed by a mechanical pump (Leybold, Trivac D4B) provided a 2×10^{-9} Torr base pressure measured by a Bayard-Alpert ionization gauge ($10^{-10}-10^{-3}$ Torr range) via a controller (Stanford Research system, IGC100). A tungsten grid (Alfa Aesar, 100 mesh size), which provided 64% transmittance, was used as the sample holder. The grid was fixed onto nickel clamps which were connected to the copper wires of a power supply/thermocouple feedthrough that was mounted at the end of a liquid nitrogen dewar. Controlled heating was achieved by a computer-interfaced (Labview, National Instruments) power supply and a type K thermocouple (chromel−alumel) spot welded on top of the tungsten grid. With this setup, the tungsten grid could be cooled to 90 K by liquid nitrogen and heated to 1400 K by resistive heating. Uniform glowing of the sample was observed, which suggested even heat distribution on the sample when the tungsten grid was heated above 1000 K. The sample holder was connected to a rotation stage (MDC) (∼240° rotation) and a Z translation stage (MDC) (1 in. vertical displacement). The spectrometer system and optical path up to the vacuum cell were purged continuously with nitrogen by making use of a simple tube-like attachment[25] between the KBr windows of the cell and the optical openings of the infrared spectrometer.

Nanotubes suspended in solvent were deposited directly onto the upper part of the tungsten grid to form a 1 cm × 2 cm rectangular film through a drop and dry method. These films were stable on the tungsten grid and could not even be removed with sonication. The thickness of the nanotube film was controlled to get an optical density (O.D.) of about 1 at ∼2300 cm^{-1}. The lower part of the blank tungsten grid without nanotubes was used as the reference.

FTIR Measurement. The vacuum cell was positioned into the sample compartment of a Bruker Optics Tensor 27 series FTIR spectrometer. A liquid nitrogen cooled MCT (HgCdTe) detector was used to record the infrared signal from the nanotube samples from 700 to 4000 cm^{-1} with a 4 cm^{-1} resolution. Reference spectra were taken on the blank tungsten grid before the nanotube sample scans. Five hundred scans were averaged for both the background and sample. After loading a new sample, the IR chamber was pumped to less than 10^{-8} torr overnight. A spectrum was taken at room temperature (300 K spectrum in the figures). The sample was subsequently degassed at 423 K for 2 h before a sequence of annealing experiments. During thermal annealing, the samples were kept at the desired temperature for 2 minutes. Then the power was turned off and samples were allowed to cool to 90 K, which took approximately 10 minutes. To desorb background gases which might adsorb during this cooling, the sample is subjected to another heating step to 423 K at 2 K/s. Spectra were taken at 90 K after the second heating.

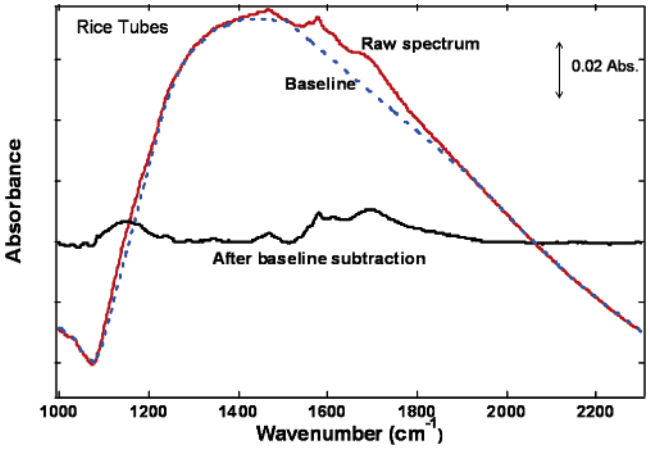

Figure 1. An example of the baseline subtraction: Rice Tubes after 700 K treatment.

To show the spectra clearly, manual baseline subtractions were applied in the data analysis of this study, using Bruker OPUS software. The baseline was a series of straight lines. An example of the baseline subtraction for the samples made by the laser-ablation technique after a 700 K treatment is shown in Figure 1.

Raman Measurement. A Nicolet Almega Dispersive Raman System with a 532 nm excitation source was used to obtain the Raman spectra. The samples were deposited on a W grid. Estimated resolution was 6−10 cm^{-1} over the spectral range of 100−4000 cm^{-1}. The Raman signal was collected by using a 1 s acquisition time, which is then summed over 30−50 acquisitions.

Results and Discussions

Stability of Oxygen-Containing Functionalities during Vacuum Heating. The infrared spectra of the as-received HiPco materials are shown in Figure 2. The broad peak around 1700 cm^{-1} is assigned to the C═O vibration of carboxylic acid groups.[20] Features assigned to C═C vibrations around 1600 cm^{-1} and C−O bands around 1150 cm^{-1} are also seen in the spectrum before heating.[20] Heating the sample to 1300 K does not create any significant change in the infrared spectrum. A similar result has been noted for this sample after vacuum heating to 700 K.[21]

Infrared spectra for the air/HCl treated HiPco samples do not show any significant differences from the as-received HiPco samples (Figure 2). This finding indicates that the air/HCl purification procedure does not introduce any detectable functionality onto the sample. The lack of functionality on the air/HCl treated tubes is most likely a result of the mild oxidation temperature used during the air oxidation and the mild acid used to extract the residual catalyst. Vacuum heating of the air/HCl-treated sample does not cause any observable change in the infrared spectra.

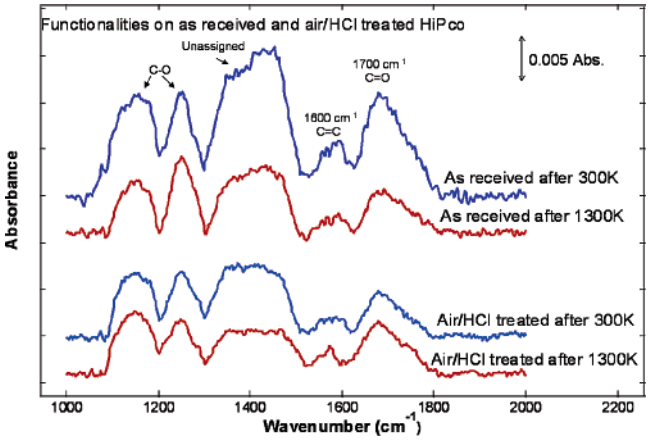

Figure 2. Evolution of IR spectra of as-received HiPco and air/HCl treated HiPco samples during vacuum heating.

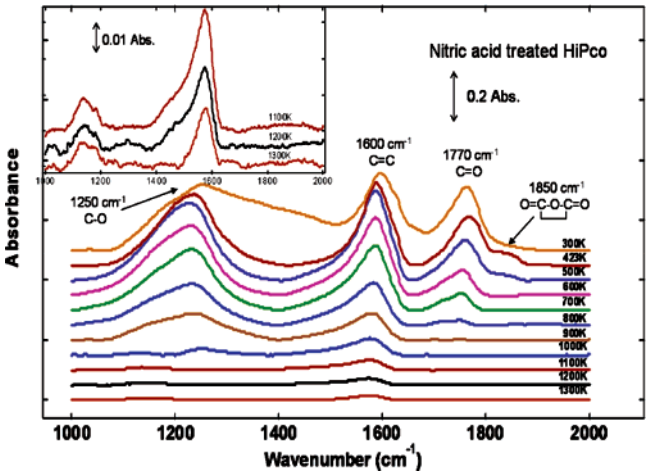

Figure 3. Evolution of IR spectra of nitric acid treated HiPco samples during vacuum heating from 300 to 1300 K.

The lack of functionalities in this sample is significant since our TGA results indicate that the air/HCl purification is as effective in reducing the metal content of samples as the other purification method studied here, HNO_3 oxidation. We also find few changes in the Raman spectra (see below) of these samples after air/HCl treatments indicating that this purification step does not introduce defects in the nanotubes sp^2 network of carbon. The results on the air/HCl-purified sample show that this procedure is highly effective in reducing metal impurities without the complication of adding functionalities or other types of defects as do other purification procedures (see below).

The infrared spectra of the nitric acid-treated HiPco samples are shown in Figure 3. The main infrared features of Figure 3 are assigned to C═O (~1770 cm^{-1}), C═C (~1600 cm^{-1}), and C−O (~1250 cm^{-1}) vibrations.[21] As noted previously,[21] the integrated intensity from these oxygen-containing functionalities is about a factor of 20 higher than what is seen in this spectral region for the as-received and air/HCl-treated HiPco samples. Since the absorbance of each sample was controlled at approximately 1 O.D. for all the samples, this intensity increase cannot be easily accounted for by sample-to-sample variations of the film thickness. Instead, it must be related to a higher density of functionalities in the HNO_3-treated sample. This high density of functionalities shows that the HNO_3 refluxing done on these samples is an effective method of functionalizing SWNTs.

The functionalities, seen in Figure 3, change drastically during thermal annealing. The carbonyl band develops a shoulder around 1850 cm^{-1} upon heating to 423 K, which we tentatively assign to a C═O stretch in a cyclic anhydride group.[26] The temperature where this change occurs (above 423 K) suggests that the anhydride may form from the coupling of two carboxylic acid groups with the loss of H_2O (dehydrolysis). The formation of anhydride functionalities is likely when the reactant groups are near each other and our observation suggests a high local density of carboxylic acid groups on the HNO_3-refluxed samples. A report by Li[27] suggests that the concentration of carboxylic acid groups is larger at the ends, the curves, and the connecting regions of SWNTs bundles.

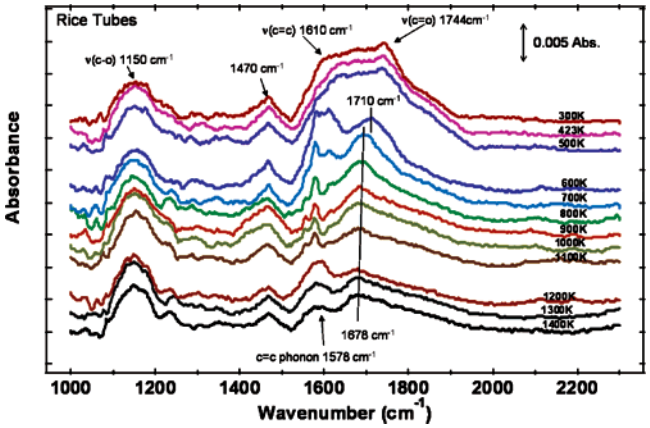

Figure 4. Evolution of IR spectra of Rice Tubes during vacuum heating from 300 to 1400 K.

The anhydride groups evidenced in Figure 3 are only observed in the nitric acid-treated HiPco sample. Due to the six-carbon ring structure of carbon nanotubes, the anhydrides should be cyclic in form, consistent with the peak seen at 1850 cm^{-1} in Figure 3. This compares with linear anhydrides which are expected to have carbonyl bands in the range from 1760 to 1820 cm^{-1}. The intensity of this 1850 cm^{-1} shoulder decreases with increasing temperature and ultimately disappears after 600 K.

The other carbonyl peak at 1770 cm^{-1} in Figure 3 also loses intensity upon heating and is completely diminished after 800 K. This change is accompanied by a frequency shift from 1770 to 1752 cm^{-1}. The band at 1597 cm^{-1}, associated with C═C bonds, decreases in intensity during heating and eventually evolves into a broad band at 1579 cm^{-1}, which is typically associated with the IR active phonon of graphitic carbons.[28] Heating to 1300 K caused the C−O functionalities to decompose, as indicated by the dramatic reduction in absorbance around 1200 cm^{-1}, leaving behind a band at around 1138 cm^{-1}. An enlargement of the spectrum for the higher temperatures (from 1100 to 1300 K) is shown as the inset of Figure 3 to highlight the residual peaks. Most of the functionalities on this sample have been removed after 1300 K heating, as shown by the IR intensity decrease seen for this spectral region.

The infrared spectra for the Rice Tubes produced by the laser-ablation technique are shown in Figure 4. Carbonyl and carbon−carbon double bond peaks are seen between 1500 and 1900 cm^{-1}. The spectra show a C−O peak at 1150 cm^{-1} and an unassigned region at ~1450 cm^{-1}.[28] Vacuum heating causes significant changes in these functionalities. The whole process can be divided into three steps:

(1) In the first step (below 500 K), the spectra do not change significantly. Only a small intensity decrease was observed for the carbonyl peak (1744 cm^{-1}) and the C═C peak (1610 cm^{-1}).

(2) In the second step (600 to 1100 K), heating causes an intensity loss of the carbonyl peak that is accompanied by a frequency shift from 1710 to 1678 cm^{-1}.[20] The peak at 1610

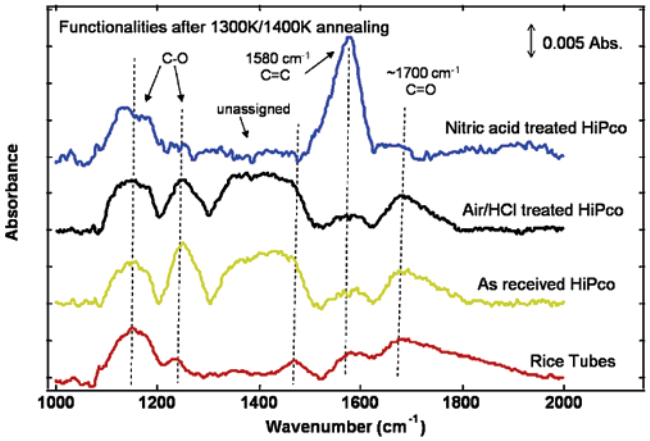

Figure 5. IR spectra of the 1000−2000 cm^{-1} region for as-received, air/HCl treated, nitric acid treated HiPco, and Rice Tubes after 1300 K/1400 K annealing.

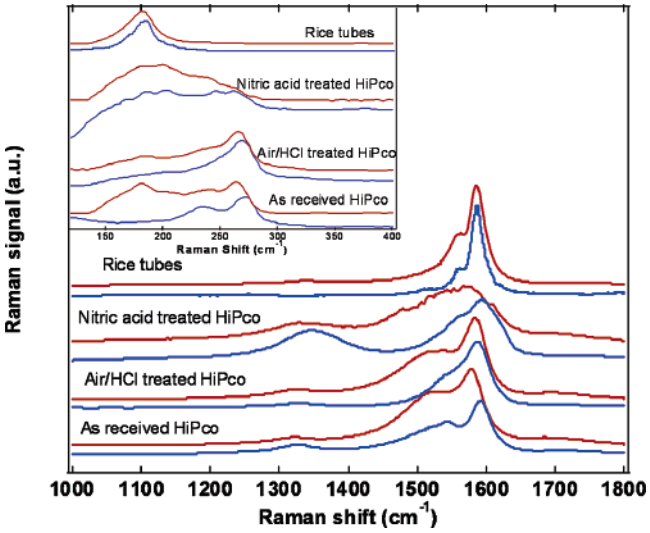

Figure 6. Raman spectra of the G band and RBM mode (inset) for as-received, air/HCl treated, nitric acid treated HiPco, and Rice Tubes both before (lower line) and after 1300 K/1400 K annealing (upper line).

cm^{-1} decreases in intensity revealing three peaks in this region at 1610, 1578, and 1556 cm^{-1}. The 1610 cm^{-1} peak has previously been assigned to intercalated NO_3^-.[29] However, this peak is not observed for the nitric acid-treated HiPco samples in this study, which possibly should also have intercalated NO_3^-.

The feature centered at 1578 cm^{-1} is similar to what is typically associated with the IR active phonon mode in nanotubes[28] and other C═C type vibrations. The features at 1556 and 1578 cm^{-1} start to merge at ∼900−1100 K and form a single, broad band near 1580 cm^{-1}. A similar behavior for the merging of these two bands was observed in a previous IR study.[28] The single broad feature formed at 1580 cm^{-1} was assigned to the IR active phonon.[28]

(3) The third step, from 1100 to 1300 K, begins with an intensity decrease of the 1470 cm^{-1} peak. A small decrease is observed for the relatively broad phonon mode at 1580 cm^{-1}. No significant change of the 1150 cm^{-1} peak occurs during the whole annealing process.

One interesting result from this work is that we find many similarities in the infrared spectra of the Rice Tubes after a 1400 K treatment with spectra for the as-received and air/HCl-treated HiPco nanotubes (Figure 5). This suggests that the heating step defunctionalizes the Rice Tubes producing a sample that is similar to the air/HCl-purified and unprocessed HiPco samples. A previous study reported that heating of acid-purified PLV (plasma laser vaporization) SWNTs produces C K-edge near edge X-ray absorption fine structure (NEXAFS) spectra which are very similar to those seen for unprocessed HiPco materials.[14] The NEXAFS result seems to agree with our infrared findings. If indeed all the functionalities are removed, then the remaining IR features should be tentatively assigned to intrinsic IR modes of the SWNTs. Further experiments and calculations will be necessary to confirm this assignment.

Ex-situ Raman spectroscopy was performed before and after the infrared experiments to check the integrity of the samples (Figure 6). The Raman spectra show G bands (∼1400−1650 cm^{-1}) and radial breathing modes (RBMs) (<350 cm^{-1}) for each sample indicating that the overall SWNT structure is intact both before and after the infrared experiments. Most of the changes with the G bands caused by purification and heating are subtle with the exception of the HNO_3-treated HiPco sample, which shows drastic broadening in comparison with the as-received HiPco sample. This change was also noted in recent work.[21,30] Associated with this is a drastic intensity increase in the D band near 1350 cm^{-1}. This D band intensity increase is consistent with the disruption of the sp^2 network of the SWNT sidewalls and is likely caused by sidewall functionalization during the HNO_3 oxidation step as evidenced in the infrared spectra of Figure 3.

Overall, the Raman data presented in Figure 6 show conclusively that the tubular structure of the samples is not disrupted by the purification or vacuum heating steps of the experiments. This indicates that the IR spectra presented here likely occur from functionalities on the nanotubes and not on some other form of carbon impurity present in the sample.

Trapped CO_2. The IR detection of physically trapped CO_2, which is generated by oxygen-containing functional groups during the thermolysis of nanotubes, has been reported.[20,21] The entrapment of CO_2 was suggested to involve the rearrangement of functionalities at defect sites as they decompose, locking the generated CO_2 into endohedral and interstitial pores in the bundle.[20,21] Rearrangements of the bundle itself due to the annealing effect of vacuum heating were also suggested to play a role.[20,21]

The ν_3 modes for trapped CO_2 are expected to be in the region of 2330 cm^{-1}.[20,21] The spectra of this region for as-received HiPco and air/HCl treated HiPco samples following thermal treatment did not show any peaks attributable to trapped CO_2. Since oxygen-containing functionalities are responsible for the evolution of carbon dioxide, the lower degree of functionalization of these samples may not be capable of generating trapped CO_2 in amounts that can be detected by infrared spectroscopy.[20,21]

For the nitric acid-treated HiPco sample, a peak attributable to the trapped CO_2 peak is seen at 2329 cm^{-1} just after heating the sample to 423 K (Figure 7). The peak intensity increases with each heating step, reaching a maximum at 700 K. Above 700 K, the CO_2 peak decreases, presumably because this trapped species starts to be released from the nanotubes. No trapped CO_2 was detected after 1100 K treatment. The data show that the peak intensity changes were accompanied by a frequency shift from 2329 cm^{-1} at 423 K, to 2334 cm^{-1} between 500 and 800 K, and finally to 2338 cm^{-1} between 900 and 1000 K. The peak around 2330 cm^{-1} has been tentatively assigned to CO_2 trapped in endohedral sites.[21]

The fate of the trapped carbon dioxide in the Rice Tubes during heating cycles is shown in Figure 8. The integrated IR absorbance associated with trapped CO_2 (Figure 9) gives two

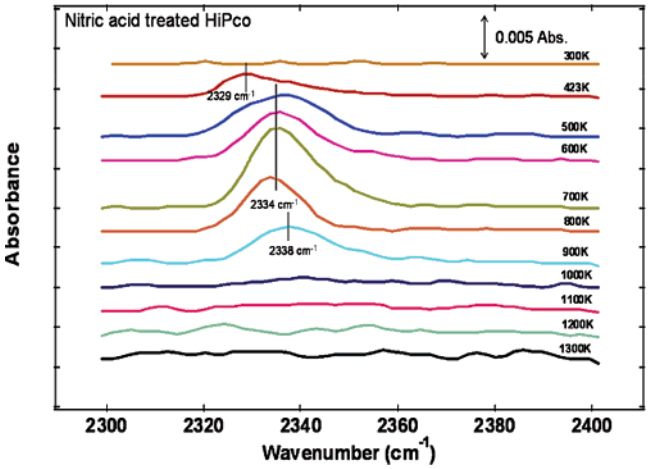

Figure 7. IR spectra for the trapped CO_2 created from the decomposition of functionalities on nitric acid treated HiPco samples.

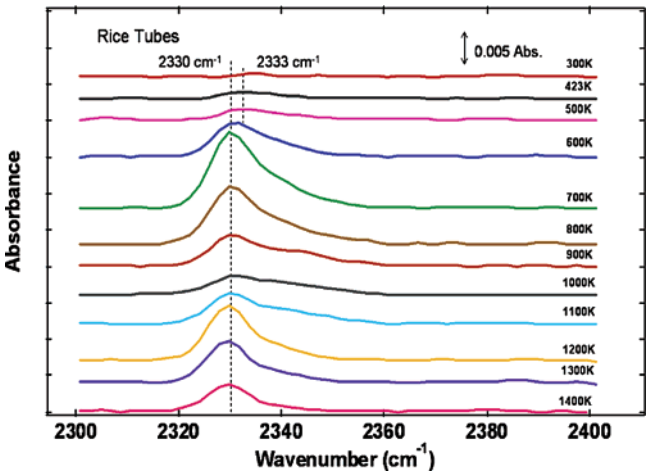

Figure 8. IR spectra for the trapped CO_2 created from the decomposition of functionalities in Rice Tubes.

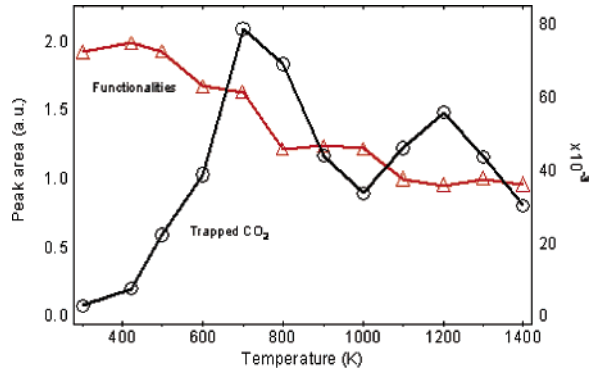

Figure 9. The integrated intensity of peaks from 1000 to 2000 cm^{-1} (in Figure 3) and trapped CO_2 peaks (in Figure 8) for Rice Tubes during thermal annealing from 300 to 1400 K.

maxima around 700 and 1100 K. The appearance of trapped CO_2 can be correlated with the decomposition of oxygen-containing functionalities as shown by the IR intensity decrease between 1000 and 2000 cm^{-1} (Figure 9). Previous IR and NEXAFS studies found that COOH group disappear below 650 K and that the C−O−C group is stable to a higher temperature (more than 1073 K).[14] Previous infrared and temperature-programmed desorption work has seen a maximum in functional group decomposition between 623 and 723 K, consistent with the results presented in Figures 8 and 9.[28]

In Figure 8, the ν_3 mode at 2330 cm^{-1} has been attributed to CO_2 in endohedral sites.[20,21] There is a high-energy tail extending up to 2340 cm^{-1}, which indicates that other adsorption sites might be populated. The peak at 2340 cm^{-1} has been attributed to CO_2 trapped in large interstitial spaces.[20] Even after a 1400 K annealing, CO_2 is not completely removed from the Rice Tubes, evidenced by the peak remaining at 2330 cm^{-1}, suggesting that there is a high-energy barrier preventing its release. It has been suggested that steric rearrangements of functionalities responsible for generating the trapped CO_2 are responsible for locking it into the nanotubes.[20,21] These functionalities could provide such a barrier.

Conclusions

The following is a summary of the main findings of our study.

(1) Nitric acid oxidation/purification generates functionalities and defects sites on nanotube surfaces. Vacuum heating decomposes most of those groups. The as-received HiPco sample has less functionality than the nitric acid-treated HiPco sample. Nitric acid refluxing is a highly effective method of oxygen functionalization.

(2) Vacuum heating of nitric acid-treated HiPco sample appears to lead to the formation of cyclic anhydride groups as indicated by the appearance of spectral features in the 1850 cm^{-1} region. The cyclic anhydride group decomposed and ultimately disappeared after thermal annealing to 600 K.

(3) Air/HCl treatment is a relatively mild purification method. The iron content decreased from 18 to 5% after purification. However, there is not much difference between as-received and air/HCl-treated HiPco infrared spectra. This shows that the air/HCl purification is highly effective in reducing metal impurities without the complication of adding functionalities or other types of defects as do other purification procedures.

(4) There are many similarities in the infrared spectra of the Rice Tubes after 1400 K treatment with spectra for the as-received and air/HCl-treated HiPco nanotubes.

(5) The drastic increase in the D band near 1350 cm^{-1} for the nitric acid-treated HiPco spectrum is consistent with the disruption of the sp^2 network of the SWNT sidewalls caused by the HNO_3 oxidation step. Thermal annealing under vacuum conditions leads to a recovery of the as-received tube character.

(6) The RBM data show that the tubular structure of the nanotube samples is not disrupted by the purification or the vacuum heating steps of the experiments.

(7) The trapped CO_2 is completely released from nitric acid-treated HiPco after 1100 K treatment. However, the existence of CO_2 in Rice Tubes after 1400 K treatment suggests the existence of a high-energy desorption barrier and the influence of production methods and purification process on their adsorption abilities.

Acknowledgment. This work was funded by the NSF (BES 0202015). The authors thank Dr. Milton Smith from Bethany College and the National Energy Technology Laboratory for help with the air/HCl purification of SWNTs. Reference in this work to any specific commercial product is to facilitate understanding and does not necessarily imply endorsement by the United States Department of Energy or the National Science Foundation.

References and Notes

(1) Kuzmany, H.; Kukovecz, A.; Simon, F.; Holzweber, A.; Kramberger, C.; Pichler, T. *Synth. Met.* **2004**, *141*, 113.

(2) Collins, P. G.; Bradley, K.; Ishigami, M.; Zettl, A. *Science* **2000**, *287*, 1801.

(3) Zhao, J. J.; Park, H. K.; Han, J.; Lu, J. P. *J. Phys. Chem. B* **2004**, *108*, 4227.

(4) Boul, P. J.; Liu, J.; Mickelson, E. T.; Huffman, C. B.; Ericson, L. M.; Chiang, I. W.; Smith, K. A.; Colbert, D. T.; Hauge, R. H.; Margrave, J. L.; Smalley, R. E. *Chem. Phys. Lett.* **1999**, *310*, 367.

(5) Halicioglu, T.; Jaffe, R. L. *Nano Lett.* **2002**, *2*, 573.

(6) Sun, Y. P.; Huang, W. J.; Lin, Y.; Fu, K. F.; Kitaygorodskiy, A.; Riddle, L. A.; Yu, Y. J.; Carroll, D. L. *Chem. Mater.* **2001**, *13*, 2864.

(7) Yang, C. M.; Kanoh, H.; Kaneko, K.; Yudasaka, M.; Iijima, S. *J. Phys. Chem. B* **2002**, *106*, 8994.

(8) Toebes, M. L.; Prinsloo, F. F.; Bitter, J. H.; van Dillen, A. J.; de Jong, K. P. *J. Catal.* **2003**, *214*, 78.

(9) Liu, C. G.; Liu, M.; Wang, M. Z.; Cheng, H. M. *New Carbon Mater.* **2002**, *17*, 64.

(10) Hafner, J. H.; Cheung, C. L.; Woolley, A. T.; Lieber, C. M. *Prog. Biophys. Mol. Biol.* **2001**, *77*, 73.

(11) Wong, S. S.; Joselevich, E.; Woolley, A. T.; Cheung, C. L.; Lieber, C. M. *Nature* **1998**, *394*, 52.

(12) Yang, Y. L.; Zhang, J.; Nan, X. L.; Liu, Z. F. *Gaodeng Xuexiao Huaxue Xuebao* **2002**, *23*, 469.

(13) Nguyen, C. V.; Delzeit, L.; Cassell, A. M.; Li, J.; Han, J.; Meyyappan, M. *Nano Lett.* **2002**, *2*, 1079.

(14) Kuznetsova, A.; Popova, I.; Yates, J. T.; Bronikowski, M. J.; Huffman, C. B.; Liu, J.; Smalley, R. E.; Hwu, H. H.; Chen, J. G. G. *J. Am. Chem. Soc.* **2001**, *123*, 10699.

(15) Zhang, J.; Zou, H. L.; Qing, Q.; Yang, Y. L.; Li, Q. W.; Liu, Z. F.; Guo, X. Y.; Du, Z. L. *J. Phys. Chem. B* **2003**, *107*, 3712.

(16) Bower, C.; Kleinhammes, A.; Wu, Y.; Zhou, O. *Chem. Phys. Lett.* **1998**, *288*, 481.

(17) Yang, C. M.; Kaneko, K.; Yudasaka, M.; Iijima, S. *Nano Lett.* **2002**, *2*, 385.

(18) Hernadi, K.; Siska, A.; Thien-Nga, L.; Forro, L.; Kiricsi, I. *Solid State Ionics* **2001**, *141*, 203.

(19) Chiang, I. W.; Brinson, B. E.; Smalley, R. E.; Margrave, J. L.; Hauge, R. H. *J. Phys. Chem. B* **2001**, *105*, 1157.

(20) Matranga, C.; Chen, L.; Smith, M.; Bittner, E.; Johnson, J. K.; Bockrath, B. *J. Phys. Chem. B* **2003**, *107*, 12930.

(21) Matranga, C.; Bockrath, B. *J. Phys. Chem. B* **2004**, *108*, 6170.

(22) Chiang, I. W.; Brinson, B. E.; Huang, A. Y.; Willis, P. A.; Bronikowski, M. J.; Margrave, J. L.; Smalley, R. E.; Hauge, R. H. *J. Phys. Chem. B* **2001**, *105*, 8297.

(23) Thess, A.; Lee, R.; Nikolaev, P.; Dai, H. J.; Petit, P.; Robert, J.; Xu, C. H.; Lee, Y. H.; Kim, S. G.; Rinzler, A. G.; Colbert, D. T.; Scuseria, G. E.; Tomanek, D.; Fischer, J. E.; Smalley, R. E. *Science* **1996**, *273*, 483.

(24) Smith, M. R.; Hedges, S. W.; LaCount, R.; Kern, D.; Shah, N.; Huffman, G. P.; Bockrath, B. *Carbon* **2003**, *41*, 1221.

(25) Wingrave, J. A.; Teplyakov, A. V. *J. Vac. Sci. Technol. A* **2003**, *21*, 1800.

(26) Nakanishi, K. *Infrared absorption spectroscopy−practical*; Holden-Day Inc.: San Francisco, CA; Nankodo Company Limited: Tokyo, Japan, 1962.

(27) Li, X. H.; Niu, J. L.; Zhang, J.; Li, H. L.; Liu, Z. F. *J. Phys. Chem. B* **2003**, *107*, 2453.

(28) Kuznetsova, A.; Mawhinney, D. B.; Naumenko, V.; Yates, J. T.; Liu, J.; Smalley, R. E. *Chem. Phys. Lett.* **2000**, *321*, 292.

(29) Hennrich, F.; Wellmann, R.; Malik, S.; Lebedkin, S.; Kappes, M. M. *Phys. Chem. Chem. Phys.* **2003**, *5*, 178.

(30) Furtado, C. A.; Kim, U. J.; Gutierrez, H. R.; Pan, L.; Dickey, E. C.; Eklund, P. C. *J. Am. Chem. Soc.* **2004**, *126*, 6095.